



## OPEN ACCESS

EDITED BY  
Mariana Frank,  
Concordia University, Canada

REVIEWED BY  
Qiang Yuan,  
Purple Mountain Observatory (CAS), China  
Vera Sinitsyna,  
Institute of Physics. PN Lebedev (RAS),  
Russia

\*CORRESPONDENCE  
Jia-Shu Niu,  
jsniu@sxu.edu.cn

SPECIALTY SECTION  
This article was submitted to High-Energy  
and Astroparticle Physics,  
a section of the journal Frontiers in  
Astronomy and Space Sciences

RECEIVED 14 September 2022  
ACCEPTED 26 October 2022  
PUBLISHED 11 November 2022

CITATION  
Niu JS and Liu J (2022), Quantitative study  
of the hardening in the Alpha Magnetic  
Spectrometer nuclei spectra at a few  
hundred GV.  
*Front. Astron. Space Sci.* 9:1044225.  
doi: 10.3389/fspas.2022.1044225

COPYRIGHT  
© 2022 Niu and Liu. This is an open-access  
article distributed under the terms of the  
[Creative Commons Attribution License \(CC  
BY\)](https://creativecommons.org/licenses/by/4.0/). The use, distribution or reproduction in  
other forums is permitted, provided the  
original author(s) and the copyright  
owner(s) are credited and that the original  
publication in this journal is cited, in  
accordance with accepted academic  
practice. No use, distribution or  
reproduction is permitted which does not  
comply with these terms.

# Quantitative study of the hardening in the Alpha Magnetic Spectrometer nuclei spectra at a few hundred GV

Jia-Shu Niu<sup>1,2\*</sup> and Jing Liu<sup>1</sup>

<sup>1</sup>Institute of Theoretical Physics, Shanxi University, Taiyuan, China, <sup>2</sup>State Key Laboratory of Quantum Optics and Quantum Optics Devices, Shanxi University, Taiyuan, China

The most significant feature in the cosmic-ray (CR) nuclei spectra is the spectral hardening at a few hundred GV. It is important to know whether the hardening of different nuclei species is the same or not for constructing CR sources and propagation models. In this work, we collect the recently released AMS-02 CR nuclei spectra of primary species (proton, helium, carbon, oxygen, neon, magnesium, silicon, and iron), secondary species (lithium, beryllium, boron, and fluorine), and hybrid species (nitrogen, sodium, and aluminum) and study the break positions and the spectral index differences (less and greater than the break rigidity) of the spectral hardening quantitatively. The results show us that the CR nuclei spectral hardening at a few hundred GV has hybrid origins. In detail, the dominating factors of the spectral hardening for primary and secondary CR nuclei species are different: the former comes from the superposition of different kinds of CR sources, while the latter comes from the propagation process. Both of these factors influence all kinds of CR nuclei spectra, just with different weights.

## KEYWORDS

galactic cosmic rays, cosmic ray propagation, origin of cosmic ray, cosmic ray energy spectrum, cosmic ray composition

## 1 Introduction

The space station experiment Alpha Magnetic Spectrometer (AMS-02) improves the measurement precision of the cosmic-ray (CR) fluxes by an order of the systematics (Aguilar and Alberti, 2013) and deepens our understanding of CRs. Based on the precision data observed by these excellent experiments represented by AMS-02, CR physics has entered a precision-driven era. More and more fine structures have been observed in CR spectra.

Until now, AMS-02 has released all the spectra of nuclei species up to the atomic number 14 (silicon) based on its first 7-year observation, including the primary CR species: proton, helium (He), carbon (C), oxygen (O), neon (Ne), magnesium (Mg), and silicon (Si) (Aguilar et al., 2021, 2020); the secondary CR species: lithium (Li), beryllium (Be), boron (B), and fluorine (F) (Aguilar et al., 2021a; Aguilar et al., 2021);

and the hybrid CR species: nitrogen (N), sodium (Na), and aluminum (Al) (Aguilar and Ali Cavazonza, 2018; 2021c). In addition, the spectrum of heavy primary species, iron (Fe), has also been released (Aguilar et al., 2021b).

From an overall perspective, the downward trends of the secondary CR species are more serious than those of the primary ones, and the hybrid ones are in the middle of both. This corresponds to the origin of the secondary CR nuclei species which are produced from collisions of primary CR particles with the interstellar medium (ISM). Most of these CR nuclei species show spectral hardening at a few hundred GV, which is the most significant feature in AMS-02 nuclei spectra. The degrees of the hardening of different CR nuclei species correspond directly to the origin of the hardening and then point to the features of CR sources and propagation models (Niu, 2021). With the accumulation of the CR event, the uncertainties in the spectra (especially in high rigidity regions) become smaller and smaller. It is both necessary and possible to carry out quantitative studies on these CR nuclei spectra, which could provide us a global view when we go further into the research on CRs.

Physically speaking, the observed CR spectra are produced by the synthetic effects of the primary source injection spectra, the propagation process, and the solar modulation; even so, it is helpful to analyze the observed CR spectra directly, which are always the starting point for building CR models. Although such kind of works have been simply performed in the AMS-02 data-released papers (Aguilar et al., 2021, 2020; Aguilar et al., 2021c), they did not always use the independent break power law formulas for different CR nuclei species (such as using one group of parameters to fit the spectral of He, C, and O and using another group of parameters to fit Ne, Mg, and Si). It would cover the differences between the CR species in one group. As a result, an independent fitting to each of the CR nuclei species *via* a uniform method could provide us not only a detailed quantitative comparison between these species but also a global view for guiding the improvements in current CR models.<sup>1</sup>

The remainder of the article is organized as follows: we first introduce the methods in Section 2; the results are shown in Section 3; and the discussions are presented in Section 4.

## 2 Materials and methods

Because the spectral hardening happens at a few hundred GV, the data points with rigidity less than 45 GV are discarded in this work. In such cases, we can avoid to handle the solar modulation and fit these CR nuclei spectra using a break power law directly.

1 Our previous work (Niu, 2021) performed similar research based on an old dataset from AMS-02, which showed large correlations of systematic errors. An updated dataset will give us more reasonable and complete results.

A break in 100–1000 GV is used to describe the position of the spectral hardening in each of the CR nuclei species.

The following formula is used to describe each of the AMS-02 nuclei spectra (including the primary CR species: proton, He, C, O, Ne, Mg, Si, and Fe; the secondary CR species: Li, Be, B, and F; and the hybrid CR species: N, Na, and Al) when the rigidity is greater than 45 GV:<sup>2</sup>

$$F^i(R) = N^i \times \begin{cases} \left(\frac{R}{R_{br}^i}\right)^{\nu_1^i} & R \leq R_{br}^i \\ \left(\frac{R}{R_{br}^i}\right)^{\nu_2^i} & R > R_{br}^i \end{cases}, \quad (1)$$

where  $F$  is the flux of CR,  $N$  is the normalization constant,  $\nu_1$  and  $\nu_2$  are the spectral indexes that are less and greater than the break rigidity  $R_{br}$ , respectively, and  $i$  denotes the species of nuclei. The errors used in our fitting are the quadratic sum of statistical and systematic errors.

The Markov chain Monte Carlo (MCMC) framework is employed to determine the posterior probability distributions (PDF) and uncertainties of the spectral parameters for different CR nuclei species.<sup>3</sup>

## 3 Results

The best-fit values and the allowed intervals from the fifth percentile to the 95th percentile of the parameters  $\nu_1$ ,  $\nu_2$ ,  $R_{br}$ , and  $\Delta\nu \equiv \nu_2 - \nu_1$  are listed in Table 1, together with the reduced  $\chi^2$  of each fitting.<sup>4</sup> The best-fit results and the corresponding residuals of the primary, the secondary, and the hybrid CR species are given in Figures 1–3, respectively.<sup>5</sup>

Generally speaking, the reduced  $\chi^2$  values of all the CR nuclei species are smaller than 1.0, which indicates the success of the break power law to describe the spectra. However, some too

2 Here, 45 GV is chosen as the rigidity cutoff conservatively because the amplitudes of the proton and He fluxes observed by AMS-02 structures decrease with the increasing rigidity and vanish above 40 GV (Aguilar et al., 2021). Similar choices can also be found in Aguilar et al. (2021).

3 The PYTHON module emcee (Foreman-Mackey et al., 2013) is employed to perform the MCMC sampling. Some such examples can be referred to Niu and Li (2018), Niu et al. (2019), and Niu (2022) and references therein.

4 The information of the parameter  $N$  is not listed in the table, which is not important in the subsequent analysis. The PDF of  $\Delta\nu \equiv \nu_2 - \nu_1$  is derived from that of  $\nu_1$  and  $\nu_2$ .

5 Note that in the lower panel of subfigures in Figures 1–3, the  $\sigma_{\text{eff}}$  is defined as

$$\sigma_{\text{eff}} = \frac{f_{\text{obs}} - f_{\text{cal}}}{\sqrt{\sigma_{\text{stat}}^2 + \sigma_{\text{syst}}^2}},$$

where  $f_{\text{obs}}$  and  $f_{\text{cal}}$  are the points which come from the observation and model calculations, respectively;  $\sigma_{\text{stat}}$  and  $\sigma_{\text{syst}}$  are the statistical and systematic standard deviations of the observed points, respectively.

TABLE 1 Fitting results of the spectral parameters for different nuclei species. Best-fit values and allowed 5th–95th percentile intervals (in the brackets) are listed for each of the parameters.

Species	$\nu_1$	$\nu_2$	$R_{br}(GV)$	$\Delta\nu$	$\chi^2/d.o.f$
Proton	−2.808 (−2.814, −2.796)	−2.671 (−2.693, −2.613)	259 (244, 348)	0.137 (0.112, 0.192)	5.95/27 = 0.22
Helium	−2.719 (−2.727, −2.709)	−2.570 (−2.602, −2.501)	367 (318, 488)	0.149 (0.115, 0.215)	3.34/28 = 0.12
Carbon	−2.727 (−2.746, −2.707)	−2.559 (−2.619, −2.479)	306 (217, 438)	0.168 (0.107, 0.245)	6.28/28 = 0.22
Oxygen	−2.694 (−2.709, −2.678)	−2.500 (−2.599, −2.392)	529 (409, 676)	0.194 (0.093, 0.306)	1.33/28 = 0.05
Neon	−2.741 (−2.759, −2.719)	−2.362 (−2.568, −2.079)	660 (542, 849)	0.379 (0.161, 0.658)	6.04/27 = 0.22
Magnesium	−2.742 (−2.765, −2.721)	−2.609 (−2.724, −2.529)	414 (323, 464)	0.133 (0.011, 0.219)	4.69/27 = 0.17
Silicon	−2.709 (−2.729, −2.690)	−2.792 (−3.299, −2.477)	923 (873, 994)	−0.083 (−0.585, 0.230)	7.21/27 = 0.27
Iron	−2.614 (−2.647, −2.573)	−2.542 (−2.756, −2.390)	392 (315, 544)	0.072 (−0.171, 0.239)	3.56/12 = 0.30
Lithium	−3.146 (−3.174, −3.109)	−2.836 (−2.905, −2.665)	216 (177, 322)	0.310 (0.239, 0.470)	17.09/27 = 0.63
Beryllium	−3.102 (−3.131, −3.066)	−2.848 (−2.967, −2.657)	247 (195, 415)	0.254 (0.122, 0.449)	12.12/27 = 0.45
Boron	−3.103 (−3.128, −3.075)	−2.765 (−2.899, −2.601)	308 (225, 436)	0.338 (0.201, 0.492)	7.31/27 = 0.27
Fluorine	−3.016 (−3.091, −2.951)	−2.844 (−3.007, −2.712)	189 (163, 216)	0.172 (−0.289, 0.347)	7.55/12 = 0.63
Nitrogen	−2.925 (−2.955, −2.883)	−2.694 (−2.753, −2.574)	199 (157, 325)	0.231 (0.158, 0.335)	15.42/27 = 0.57
Sodium	−2.913 (−2.958, −2.873)	−2.657 (−3.213, −2.372)	558 (442, 629)	0.256 (−0.293, 0.558)	1.21/12 = 0.10
Aluminum	−2.827 (−2.870, −2.785)	−2.487 (−2.733, −2.268)	401 (270, 500)	0.340 (0.076, 0.574)	2.71/12 = 0.23

small reduced  $\chi^2$  values imply an improper treatment of the data errors. The improvement in the treatment needs additional information about the correlation matrix of systematic errors of AMS-02 data. Some detailed discussions of this topic can be found in [Derome et al. \(2019\)](#), [Weinrich et al. \(2020\)](#), and [Heisig et al. \(2020\)](#). One should note that the reduced  $\chi^2$  values in [Table 1](#) do not have the absolute meaning of goodness-of-fit, although they can be compared with each other.

## 4 Discussion

In order to get a clear representation and comparison of the fitted parameters of the different nuclei species, the boxplots<sup>6</sup> of the spectral parameters are used to show the distributions of  $\nu_1$ ,  $\nu_2$ ,  $R_{br}$ , and  $\Delta\nu \equiv \nu_2 - \nu_1$  in [Figure 4](#).

In the boxplots of  $\nu_1$  in [Figure 4](#), the secondary species have the lowest values, followed by the hybrid species and the primary CR species. It is obvious that the  $\nu_1$  values of proton and Fe are significantly different from those of the other primary CR species. The former is always referred to the p/He anomaly, which is generally ascribed to the particle-dependent acceleration mechanisms occurring in galactic CR sources (see, for e.g., [Vladimirov and Johannesson \(2012\)](#)). Also, many specific mechanisms are proposed to interpret this anomaly (see, for e.g., [Erlykin and Wolfendale \(2015\)](#);

[Malkov et al. \(2012\)](#); [Fisk and Gloeckler \(2012\)](#); [Ohira and Ioka \(2011\)](#); [Tomassetti \(2015b\)](#)). The latter comes from the significantly larger interaction cross sections with the ISM of Fe than those of lighter nuclei species (He, C, O, Ne, Mg, and Si) ([Aguilar et al., 2021b](#)). For the secondary CR nuclei species, the  $\nu_1$  value of F is larger than that of others, which indicates that the propagation of heavy CRs (from F to Si) might be different from that of light CRs (from He to O). For the hybrid CR nuclei species, the  $\nu_1$  value of Al is larger than that of N and Na. This is a direct sign of its higher proportion of primary components than N and Na (see [Aguilar and Ali Cavazonza, \(2018; 2021c\)](#) for more details). One should note that a trend is implied in this subfigure: if we consider the  $\nu_1$  values in one group of CR nuclei species (primary, secondary, or hybrid), they increase with the increase in atomic numbers. Whether this trend is just a coincidence, or it comes from an undiscovered mechanism (such as a charge- or mass-dependent acceleration or propagation) should be tested in the future.

In the boxplots of  $\nu_2$  in [Figure 4](#), the uncertainties are larger than those of  $\nu_1$  because of the fewer data points with larger uncertainties in high rigidity regions. Roughly speaking, the  $\nu_2$  values of the primary CR nuclei species are larger than those of the secondary species (except those of Si with quite large uncertainties). For hybrid CR nuclei species, N has a  $\nu_2$  value with low uncertainty of about 2%, which is the same as the one for proton and within the uncertainty of the other primary species; the  $\nu_2$  uncertainty of Na is about 20%, which is similar to that of Si (about 18%–19%); the  $\nu_2$  of Al has an uncertainty of about 9%–10% and is similar to the values of the primary ones, which indicates that its flux in high rigidity regions is dominated by the primary component.

In the boxplots of  $R_{br}$  in [Figure 4](#), it shows that the break positions are significantly different between some of the CR nuclei species, especially in the case of primary and hybrid

<sup>6</sup> A box plot is a method for graphically depicting groups of numerical data through their quartiles. In our configurations, the band inside the box shows the median value of the dataset, the box shows the quartiles, and the whiskers extend to show the rest of the distribution which are edged by the fifth percentile and the 95th percentile.

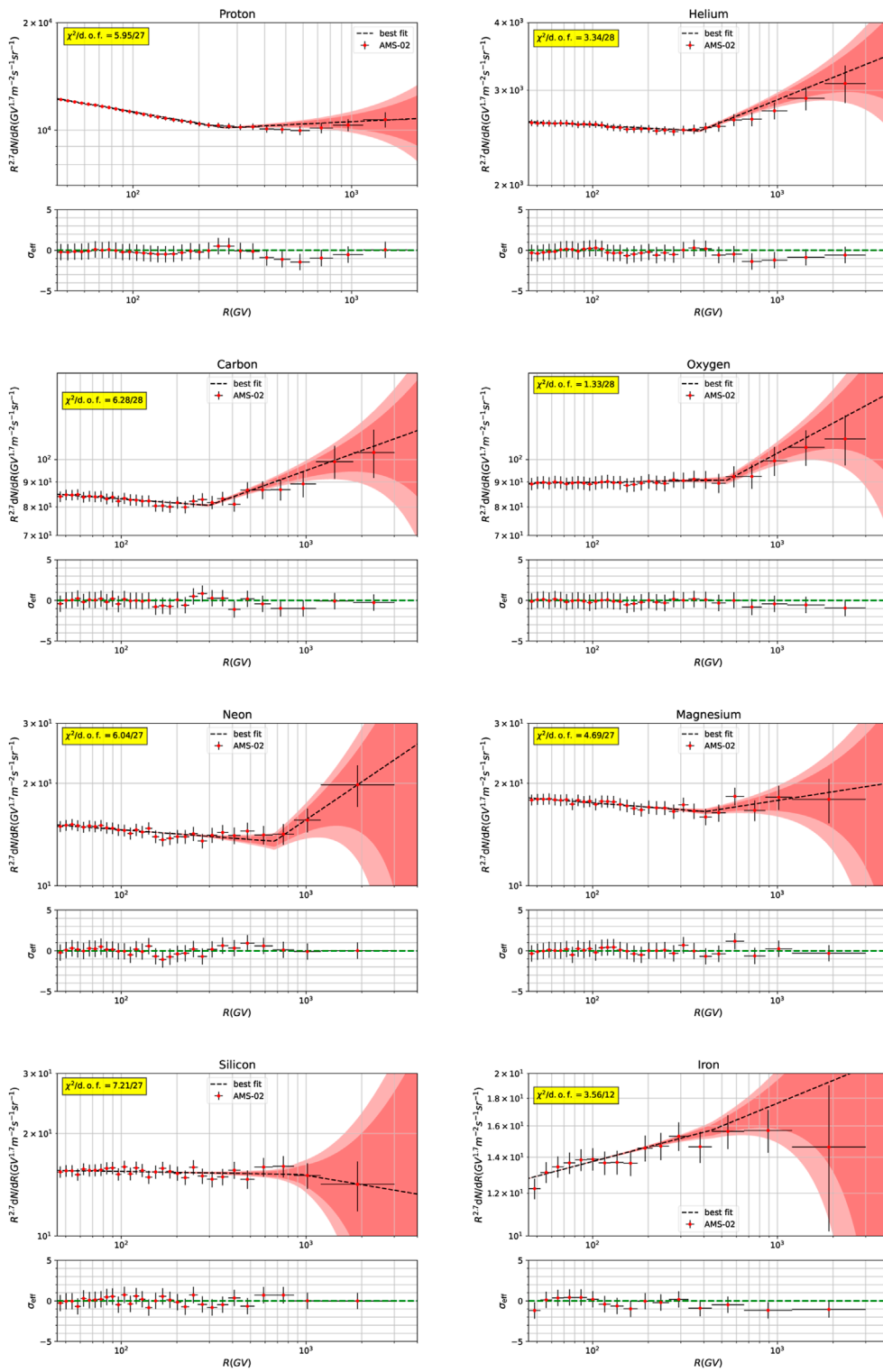
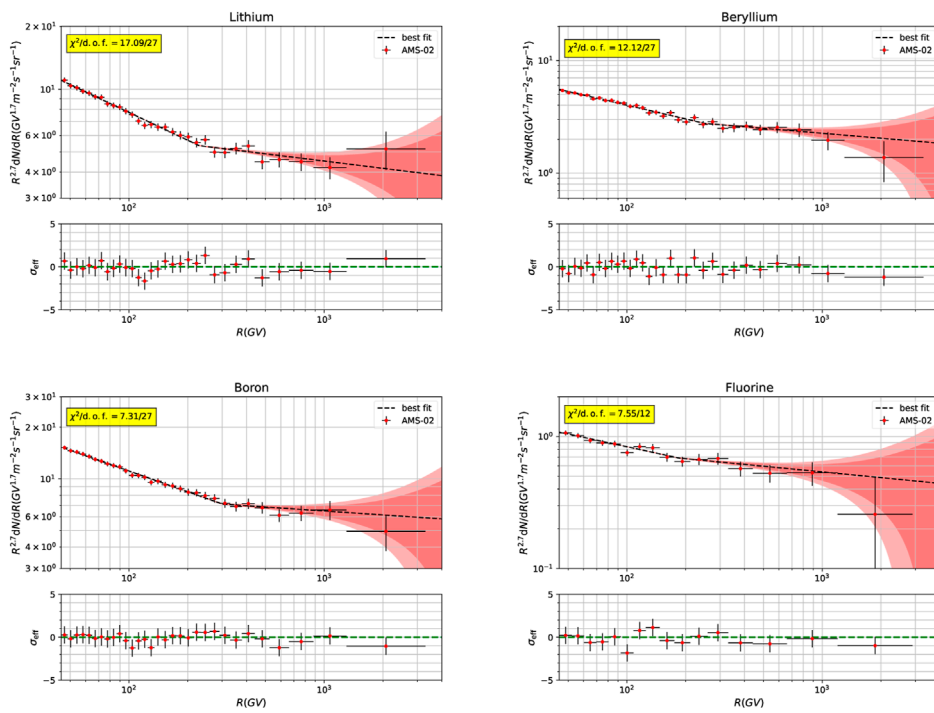
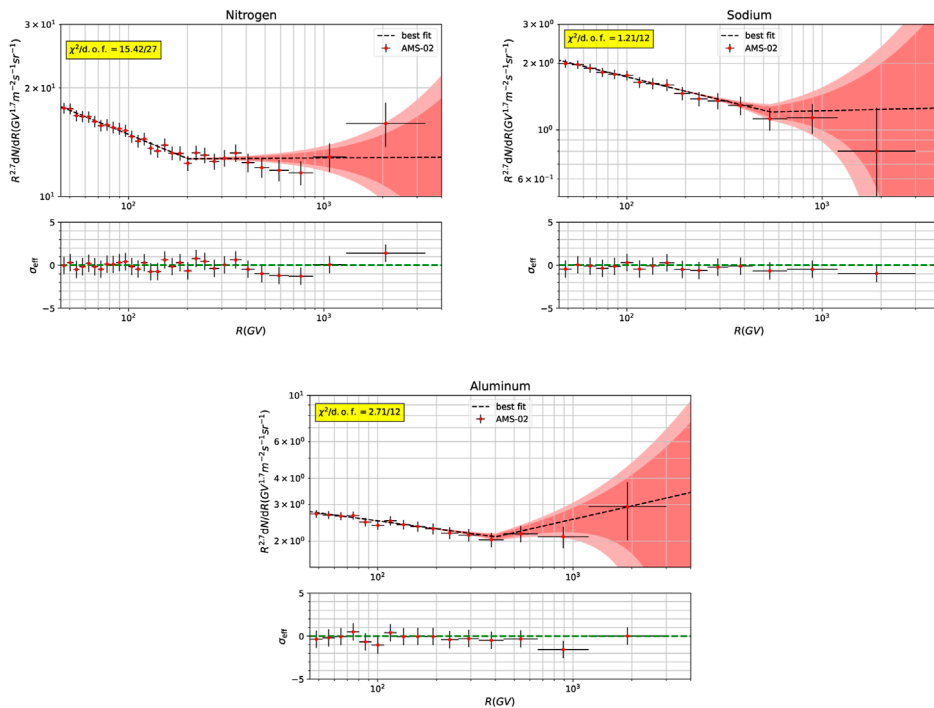


FIGURE 1

Fitting results and corresponding residuals to the primary CR nuclei spectra (proton, He, C, O, Ne, Mg, Si, and Fe). The  $2\sigma$  (deep red) and  $3\sigma$  (light red) bounds are also shown in the subfigures. The relevant reduced  $\chi^2$  value of each spectrum is given in the subfigures as well.



**FIGURE 2** Fitting results and corresponding residuals to the secondary CR nuclei spectra (Li, Be, B, and F). The  $2\sigma$  (deep red) and  $3\sigma$  (light red) bounds are also shown in the subfigures. The relevant reduced  $\chi^2$  value of each spectrum is given in the subfigures as well.



**FIGURE 3** Fitting results and corresponding residuals to the hybrid CR nuclei spectra (N, Na, and Al). The  $2\sigma$  (deep red) and  $3\sigma$  (light red) bounds are also shown in the subfigures. The relevant reduced  $\chi^2$  value of each spectrum is given in the subfigures as well.

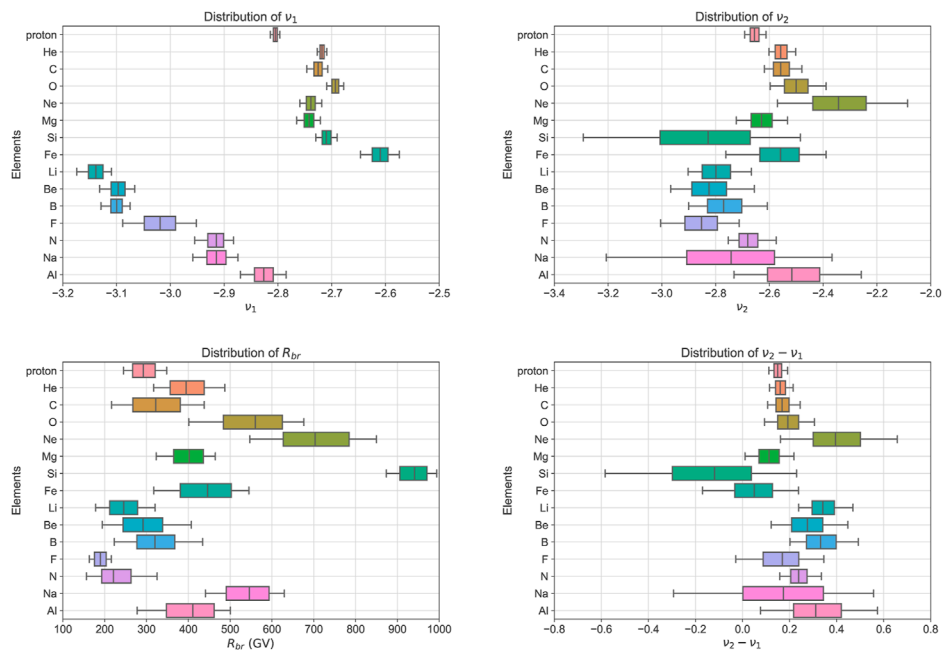


**FIGURE 4**

Boxplots for  $v_1$ ,  $v_2$ ,  $R_{br}$ , and  $v_2 - v_1 \equiv \Delta v$ . The band inside the box shows the median value of the dataset, the box shows the quartiles, and the whiskers extend to show the rest of the distribution which are edged by the fifth percentile and the 95th percentile.

species. On the contrary, the break positions of the secondary CR nuclei species are distributed around 200–400 GV, which are a bit more concentrated and indicate that they might have a common origin. If the spectral hardening of the secondary CR nuclei species (Li, Be, B, and F) mainly comes from their parents' species (C, N, O, Ne, Na, Mg, Al, and Si), their break position should have similar distributions. Considering the heavy secondary CR nuclei species F, it is thought to be produced mostly by the collisions of heavy nuclei (such as Ne, Mg, and Si) with the ISM, but its break position distributes around 200 GV, which is significantly different from its parents' species (all of them are larger than 300 GV). This is definite evidence that the spectral hardening in the secondary CR nuclei species does not predominantly inherit from their parents' species, and the main factor of their hardening comes from propagation [such as in Blasi et al. (2012); Tomassetti (2012, 2015b,a); Feng et al. (2016); Génolini and Serpico. (2017); Jin et al. (2016); Guo and Yuan (2018a,b); Liu et al. (2018); Niu et al. (2019); Boschini et al. (2020a,b); and Niu (2022)]. Moreover, such diffuse distributions of the break positions of the primary CR nuclei species cannot be predominantly reproduced by a uniform acceleration mechanism in CR sources or in propagation processes, and the superposition of different kinds of sources (with different spectral indexes and element abundances) seems to be the only natural explanation [such

as in Yuan et al. (2011); Yue and Ma. (2019); Yuan et al. (2020); Niu (2021)].

In the boxplots of  $v_2 - v_1$  in Figure 4, some of the  $\Delta v$  values inherit large uncertainties from  $v_2$ , especially for Ne, Si, Fe, Na, and Al. Generally speaking, the  $v_2 - v_1$  values are the same for primary, secondary, and hybrid species within the uncertainties. As the measurement of the spectral hardening, the  $\Delta v$  values of Si and Fe distribute around zero, which demonstrates that the spectral hardening in these two species is not statistically significant. Moreover, it shows that the  $\Delta v$  values of some primary CR nuclei species whose spectra have relatively smaller uncertainties (proton, He, C, O, and Mg) are systematically smaller than those of the secondary species Li, Be, and B, which is the reason why some precious works claimed that AMS-02 data (including the spectra or spectra ratio of Li, Be, B, C, and O) favor a break in the diffusion coefficient index rather than a break in the primary source injection [see, for e.g., Génolini and Serpico. (2017); Niu and Xue (2020)]. In addition, the  $\Delta v$  of F seems to be systematically smaller than that of Li, Be, and B. If we follow the conclusion obtained previously (the spectral hardening of the secondary CR nuclei species predominantly comes from the propagation process), it is an indication that the propagation properties of heavy cosmic rays, from F to Si, are different from those of light cosmic rays, from He to O (Aguilar et al., 2021a).

## 5 Summary

In summary, for the primary CR nuclei species, although  $v_1$  and  $v_2$  have similar values within uncertainties (except for the  $v_1$  of proton and Fe with special reasons), the significant different values of  $R_{br}$  indicate that their spectral hardening cannot come from a uniform mechanism in CR sources or propagation processes. A natural origin of the hardening is the superposition of different kinds of CR sources, which on the one hand corresponds to the galactic averaged CR sources and a local CR source [such as Geminga SNR (Zhao et al., 2022) and the superflares from nearby M dwarfs (Ohm and Hoischen, 2018)], and on the other hand corresponds to different kinds of CR factories, such as the different population of supernova remnants (Aharonian et al., 2004), galactic center (Scherer et al., 2022), novae (H.E.S.S. Collaboration, 2022), and active red dwarf stars (Sinityna et al., 2021). In both cases, as long as the CR sources have different elemental abundances, it will produce different  $v_2 - v_1$  and  $R_{br}$  values for different CR nuclei species. The combination of the aforementioned two cases is also possible (Zhang et al., 2022).

For the secondary CR nuclei species, their concentrated values of  $R_{br}$  are different from those of their parent species, which denies the possibility of the inheritance from the primary species and favors the propagation origin (such as the spatial-dependent propagation (Tomassetti, 2012; Guo et al., 2016)). Here, the different propagation regions correspond to the structures of the galaxy (i.e., the galaxy center, the bulk, the disk, the halo, and even the spiral arms), in which the densities of ISM are different, and thus they have different propagation environments.

As a result, the dominating factors of the spectral hardening for primary and secondary CR nuclei species are different. Of course, these factors will influence all the CR nuclei species spectra, regardless of the primary, the secondary, or the hybrid ones, just with different weights. The hybrid origins of the CR nuclei spectral hardening at a few hundred GV are also confirmed by Niu (2022) via a propagation model. These hybrid origins will not only produce a break at about 200 GV in secondary/primary ratios (such as B/C and B/O), which corresponds to the dominating spectral hardening for secondary species, but also produce breaks greater than 200 GV in secondary/primary ratios, which corresponds to the dominating spectral hardening for primary species. These predictions are confirmed by the recently released B/C and B/O ratios from DAMPE (DAMPE Collaboration, 2022). Moreover, the slightly different  $\Delta v$  and  $R_{br}$  distributions between F and Li/Be/B show

some hints that the propagation properties of heavy CRs are different from those of light CRs.

## Data availability statement

Publicly available datasets were analyzed in this study. These data can be found at: [doi:10.1016/j.physrep.2020.09.003](https://doi.org/10.1016/j.physrep.2020.09.003) [doi:10.1103/PhysRevLett.121.051103](https://doi.org/10.1103/PhysRevLett.121.051103) [doi:10.1103/PhysRevLett.124.211102](https://doi.org/10.1103/PhysRevLett.124.211102) [doi:10.1103/PhysRevLett.126.081102](https://doi.org/10.1103/PhysRevLett.126.081102) [doi:10.1103/PhysRevLett.126.041104](https://doi.org/10.1103/PhysRevLett.126.041104) [doi:10.1103/PhysRevLett.127.021101](https://doi.org/10.1103/PhysRevLett.127.021101).

## Author contributions

J-SN proposed the original idea and wrote the manuscript; and JL carried out some calculations.

## Funding

This research was supported by the National Natural Science Foundation of China (NSFC; Nos. 12005124 and 12147215).

## Acknowledgments

J-SN would like to thank Hui-Fang Xue and Jue-Ran Niu for providing a quiet working environment.

## Conflict of interest

The authors declare that the research was conducted in the absence of any commercial or financial relationships that could be construed as a potential conflict of interest.

## Publisher's note

All claims expressed in this article are solely those of the authors and do not necessarily represent those of their affiliated organizations, or those of the publisher, the editors, and the reviewers. Any product that may be evaluated in this article, or claim that may be made by its manufacturer, is not guaranteed or endorsed by the publisher.

## References

- Aguilar, M., Alberti, G., Alvino, A., Ambrosi, G., Andeen, K., et al. (2013). First result from the alpha magnetic spectrometer on the international space station: Precision measurement of the positron fraction in primary cosmic rays of 0.5–350 GeV. *Phys. Rev. Lett.* 110, 141102. doi:10.1103/PhysRevLett.110.141102
- Aguilar, M., Ali Cavazonza, L., Ambrosi, G., Arruda, L., Attig, N., Barao, F., et al. (2021). The alpha magnetic spectrometer (AMS) on the international space station: Part II - results from the first seven years. *Phys. Rep.* 894, 1–116. doi:10.1016/j.physrep.2020.09.003
- Aguilar, M., Ali Cavazonza, L., Ambrosi, G., Arruda, L., Attig, N., et al. (2018). Precision measurement of cosmic-ray nitrogen and its primary and secondary components with the alpha magnetic spectrometer on the international space station. *Phys. Rev. Lett.* 121, 051103. doi:10.1103/PhysRevLett.121.051103
- Aguilar, M., Cavazonza, L., Arruda, L., Attig, N., Barao, F., et al. (2020). Properties of neon, magnesium, and silicon primary cosmic rays results from the alpha magnetic spectrometer. *Phys. Rev. Lett.* 124, 211102. doi:10.1103/PhysRevLett.124.211102
- Aguilar, M., Cavazonza, L. A., Allen, M. S., Alpat, B., Ambrosi, G., Arruda, L., et al. (2021a). Properties of heavy secondary fluorine cosmic rays: Results from the alpha magnetic spectrometer. *Phys. Rev. Lett.* 126, 081102. doi:10.1103/PhysRevLett.126.081102
- Aguilar, M., Cavazonza, L. A., Allen, M. S., Alpat, B., Ambrosi, G., Arruda, L., et al. (2021b). Properties of iron primary cosmic rays: Results from the alpha magnetic spectrometer. *Phys. Rev. Lett.* 126, 041104. doi:10.1103/PhysRevLett.126.041104
- Aguilar, M., Cavazonza, L. A., Alpat, B., Ambrosi, G., Arruda, L., Attig, N., et al. (2021c). Properties of a new group of cosmic nuclei: Results from the alpha magnetic spectrometer on sodium, aluminum, and nitrogen. *Phys. Rev. Lett.* 127, 021101. doi:10.1103/PhysRevLett.127.021101
- Aharonian, F. A., Akhperjanian, A. G., Aye, K. M., Bazer-Bachi, A. R., Beilicke, M., Benbow, W., et al. (2004). High-energy particle acceleration in the shell of a supernova remnant. *Nature* 432, 75–77. doi:10.1038/nature02960
- Blasi, P., Amato, E., and Serpico, P. D. (2012). Spectral breaks as a signature of cosmic ray induced turbulence in the galaxy. *Phys. Rev. Lett.* 109, 061101. doi:10.1103/PhysRevLett.109.061101
- Boschini, M. J., Della Torre, S., Gervasi, M., Grandi, D., Jóhannesson, G., La Vacca, G., et al. (2020a). Deciphering the local interstellar spectra of secondary nuclei with the galprop/helmod framework and a hint for primary lithium in cosmic rays. *Astrophys. J.* 889, 167. doi:10.3847/1538-4357/ab64f1
- Boschini, M. J., Della Torre, S., Gervasi, M., Grandi, D., Jóhannesson, G., La Vacca, G., et al. (2020b). Inference of the local interstellar spectra of cosmic-ray nuclei  $Z \leq 28$  with the GALPROP-HELMOD framework. *Astrophys. J. Suppl. Ser.* 250, 27. doi:10.3847/1538-4365/aba901
- DAMPE Collaboration (2022). Detection of spectral hardenings in cosmic-ray boron-to-carbon and boron-to-oxygen flux ratios with dampe. *Sci. Bull.* doi:10.1016/j.scib.2022.10.002
- Derome, L., Maurin, D., Salati, P., Boudaud, M., Génolini, Y., and Kunzé, P. (2019). Fitting B/C cosmic-ray data in the AMS-02 era: A cookbook. Model numerical precision, data covariance matrix of errors, cross-section nuisance parameters, and mock data. *Astron. Astrophys.* 627, A158. doi:10.1051/0004-6361/201935717
- Erykin, A. D., and Wolfendale, A. W. (2015). The spectral shapes of hydrogen and helium nuclei in cosmic rays. *J. Phys. G. Nucl. Part. Phys.* 42, 075201. doi:10.1088/0954-3899/42/7/075201
- Feng, J., Tomassetti, N., and Oliva, A. (2016). Bayesian analysis of spatial-dependent cosmic-ray propagation: Astrophysical background of antiprotons and positrons. *Phys. Rev. D.* 94, 123007. doi:10.1103/PhysRevD.94.123007
- Fisk, L. A., and Gloeckler, G. (2012). Acceleration of galactic cosmic rays in the interstellar medium. *Astrophys. J.* 744, 127. doi:10.1088/0004-637X/744/2/127
- Foreman-Mackey, D., Hogg, D. W., Lang, D., and Goodman, J. (2013). emcee: The MCMC Hammer. *Publ. Astron. Soc. Pac.*, 125, 306. doi:10.1086/670067
- Génolini, Y., Serpico, P. D., Caroff, S., Poulin, V., Derome, L., et al. (2017). Indications for a high-rigidity break in the cosmic-ray diffusion coefficient. *Phys. Rev. Lett.* 119, 241101. doi:10.1103/PhysRevLett.119.241101
- Guo, Y.-Q., Tian, Z., and Jin, C. (2016). Spatial-dependent propagation of cosmic rays results in spectrum of proton, ratios of  $\bar{P}/P$ , B/C and anisotropy of nuclei. *Astrophys. J.* 819, 54. doi:10.3847/0004-637X/819/1/54
- Guo, Y.-Q., and Yuan, Q. (2018a). On the knee of Galactic cosmic rays in light of sub-TeV spectral hardenings. *Chin. Phys. C* 42, 075103. doi:10.1088/1674-1137/42/7/075103
- Guo, Y.-Q., and Yuan, Q. (2018b). Understanding the spectral hardenings and radial distribution of Galactic cosmic rays and Fermi diffuse  $\gamma$  rays with spatially-dependent propagation. *Phys. Rev. D.* 97, 063008. doi:10.1103/PhysRevD.97.063008
- Heisig, J., Korsmeier, M., and Winkler, M. W. (2020). Dark matter or correlated errors: Systematics of the AMS-02 antiproton excess. *Phys. Rev. Res.* 2, 043017. doi:10.1103/PhysRevResearch.2.043017
- H.E.S.S. Collaboration, Ait Benkhali, F., Anguner, E. O., Ashkar, H., Backes, M., Baghmany, V., et al. (2022). Time-resolved hadronic particle acceleration in the recurrent nova rs ophiuchi. *Science* 10, 77–80. doi:10.1126/science.abn0567
- Jin, C., Guo, Y.-Q., and Hu, H.-B. (2016). Spatial dependent diffusion of cosmic rays and the excess of primary electrons derived from high precision measurements by AMS-02. *Chin. Phys. C* 40, 015101. doi:10.1088/1674-1137/40/1/015101
- Liu, W., Yao, Y.-h., and Guo, Y.-Q. (2018). Revisiting the spatially dependent propagation model with the latest observations of cosmic-ray nuclei. *Astrophys. J.* 869, 176. doi:10.3847/1538-4357/aaef39
- Malkov, M. A., Diamond, P. H., and Sagdeev, R. Z. (2012). Proton-helium spectral anomaly as a signature of cosmic ray accelerator. *Phys. Rev. Lett.* 108, 081104. doi:10.1103/PhysRevLett.108.081104
- Niu, J.-S. (2022). Hybrid origins of the cosmic-ray nucleus spectral hardening at a few hundred GV. *Astrophys. J.* 932, 37. doi:10.3847/1538-4357/ac6d5a
- Niu, J.-S., and Li, T. (2018). Galactic cosmic-ray model in the light of AMS-02 nuclei data. *Phys. Rev. D.* 97, 023015. doi:10.1103/PhysRevD.97.023015
- Niu, J.-S., Li, T., and Xue, H.-F. (2019). Bayesian analysis of the hardening in AMS-02 nuclei spectra. *Astrophys. J.* 873, 77. doi:10.3847/1538-4357/ab0420
- Niu, J.-S. (2021). Origin of hardening in spectra of cosmic ray nuclei at a few hundred GeV using AMS-02 data. *Chin. Phys. C* 45, 041004. doi:10.1088/1674-1137/abe03d
- Niu, J.-S., and Xue, H.-F. (2020). Some new hints on cosmic-ray propagation from AMS-02 nuclei spectra. *J. Cosmol. Astropart. Phys.* 2020, 036. doi:10.1088/1475-7516/2020/01/036
- Ohira, Y., and Ioka, K. (2011). Cosmic-ray helium hardening. *Astrophys. J.* 729, L13. doi:10.1088/2041-8205/729/1/L13
- Ohm, S., and Hoischen, C. (2018). On the expected  $\gamma$ -ray emission from nearby flaring stars. *Mon. Not. R. Astron. Soc.* 474, 1335–1341. doi:10.1093/mnras/stx2806
- Scherer, A., Cuadra, J., and Bauer, F. E. (2022). Galactic center gamma-ray production by cosmic rays from stellar winds and Sgr A East. *Astron. Astrophys.* 659, A105. doi:10.1051/0004-6361/202142401
- Sinitsyna, V. G., Sinitsyna, V. Y., and Stozhkov, Y. I. (2021). Red dwarf stars as a new source type of galactic cosmic rays. *Astron. Nachr.* 342, 342–346. doi:10.1002/asna.202113931
- Tomassetti, N. (2015a). Cosmic-ray protons, nuclei, electrons, and antiparticles under a two-halo scenario of diffusive propagation. *Phys. Rev. D.* 92 (R), 081301. doi:10.1103/PhysRevD.92.081301
- Tomassetti, N. (2012). Origin of the cosmic-ray spectral hardening. *Astrophys. J.* 752, L13. doi:10.1088/2041-8205/752/1/L13
- Tomassetti, N. (2015b). Origin of the proton-to-helium ratio anomaly in cosmic rays. *Astrophys. J.* 815, L1. doi:10.1088/2041-8205/815/1/L1
- Vladimirov, A. E., Jóhannesson, G., Porter, T. A., et al. (2012). Testing the origin of high-energy cosmic rays. *Astrophys. J.* 752, 68. doi:10.1088/0004-637X/752/1/68
- Weinrich, N., Génolini, Y., Boudaud, M., Derome, L., and Maurin, D. (2020). Combined analysis of AMS-02 (Li, Be, B)/C, N/O,  $^3\text{He}$ , and  $^4\text{He}$  data. *Astron. Astrophys.* 639, A131. doi:10.1051/0004-6361/202037875
- Yuan, Q., Qiao, B.-Q., Guo, Y.-Q., Fan, Y.-Z., and Bi, X.-J. (2020). Nearby source interpretation of differences among light and medium composition spectra in cosmic rays. *Front. Phys. (Beijing)*, 16, 24501. doi:10.1007/s11467-020-0990-4
- Yuan, Q., Zhang, B., and Bi, X.-J. (2011). Cosmic ray spectral hardening due to dispersion in the source injection spectra. *Phys. Rev. D.* 84, 043002. doi:10.1103/PhysRevD.84.043002
- Yue, C., Ma, P.-X., Fan, Y. Z., Chen, Z. F., Cui, M. Y., et al. (2019). Implications on the origin of cosmic rays in light of 10 TV spectral softenings. *Front. Phys. (Beijing)*, 15, 24601. doi:10.1007/s11467-019-0946-8
- Zhang, Y., Liu, S., and Zeng, H. (2022). A three-component model for cosmic ray spectrum and dipole anisotropy. *Mon. Not. R. Astron. Soc.* 511, 6218–6224. doi:10.1093/mnras/stac470
- Zhao, B., Liu, W., Yuan, Q., Hu, H.-B., Bi, X.-J., Wu, H.-R., et al. (2022). Geminga SNR: Possible candidate of the local cosmic-ray factory. *Astrophys. J.* 926, 41. doi:10.3847/1538-4357/ac4416